




LINC00997/MicroRNA 574-3p/CUL2 Promotes Cervical Cancer Development via Mitogen-Activated Protein Kinase Signaling

Daming Chu,^a Tengteng Liu,^a Yuan Yao,^b  Nannan Luan^a

^aDepartment of Obstetrics and Gynecology, Shengjing Hospital of China Medical University, Shenyang, Liaoning, China

^bDepartment of Oncology, The People's Hospital of Liaoning Province, Shenyang, Liaoning, China

ABSTRACT Cervical cancer (CC) is a common gynecological malignancy with high morbidity and mortality. Mounting evidence has highlighted that long noncoding RNAs are essential regulators in cancer development. Long intergenic non-protein-coding RNA 997 (LINC00997) was identified for study due to its high expression in CC tissues. The aim of the study was to investigate the function and mechanism of LINC00997 in CC. Reverse transcription-quantitative PCR (RT-qPCR) revealed that LINC00997 RNA expression was also increased in CC cells and LINC00997 copy number was upregulated in CC tissues. 3-(4,5-Dimethyl-2-thiazolyl)-2,5-diphenyl-2H-tetrazolium bromide (MTT), colony formation, and Transwell assays as well as transmission electron microscopy observation exhibited that LINC00997 depletion inhibited CC cell proliferation, migration, invasion, and autophagy. The relationship between LINC00997 and its downstream genes was confirmed by RNA pulldown, luciferase reporter, and RNA-binding protein immunoprecipitation assays. Mechanistically, LINC00997 upregulated the expression of cullin 2 (CUL2) by interacting with microRNA 574-3p (miR-574-3p). Moreover, Western blot analysis was employed to detect the protein levels of mitogen-activated protein kinase (MAPK) pathway-associated factors in CC cells. LINC00997 activated the MAPK signaling by increasing CUL2 expression, thus promoting malignant phenotypes of CC cells. In conclusion, the LINC00997/miR-574-3p/CUL2 axis contributes to CC cell proliferation, migration, invasion, and autophagy via the activation of MAPK signaling.

KEYWORDS LINC00997, miR-574-3p, CUL2, MAPK signaling, cervical cancer, ERK/MAPK

Cervical cancer (CC) is a prevalent tumor with the 4th highest incidence in women globally (1), and it was responsible for approximately 570,000 cases and 311,000 deaths in 2018 (2). Surgical resection, radiotherapy, and chemotherapy are available therapeutic methods for CC treatment. However, the long-term prognosis of CC patients is still poor due to the high recurrence of CC or clinical resistance in cancer therapy (3–5). Over the last few decades, molecular targeted therapies for cancer have become increasingly important. To improve the prognosis of patients with CC and enrich therapeutic options, it is necessary to explore mechanisms underlying the initiation and development of CC.

Long noncoding RNAs (lncRNAs) are transcripts of more than 200 nucleotides in length, acting as critical noncoding RNAs in biological processes, including epigenetic regulation, cell development, and transcriptional regulation (6, 7). Importantly, the biological role of lncRNAs in CC development has been widely reported. For example, lncRNA plasmacytoma variant translocation 1 (PVT1) promotes CC cell migration and invasion by decreasing the expression of microRNA 424 (miR-424) (8). lncRNA C5orf66 antisense RNA 1 (C5orf66-AS1) enhances cell proliferation, restrains cell apoptosis, and promotes tumor growth in CC (9). Mechanistically, multiple lncRNAs were found to serve as competing endogenous RNAs (ceRNAs) in CC development (10, 11). Under the ceRNA mechanism, lncRNAs interact with microRNAs (miRNAs) to stabilize the expression of

Citation Chu D, Liu T, Yao Y, Luan N. 2021. LINC00997/microRNA 574-3p/CUL2 promotes cervical cancer development via mitogen-activated protein kinase signaling. *Mol Cell Biol* 41:e00059-21. <https://doi.org/10.1128/MCB.00059-21>.

Copyright © 2021 American Society for Microbiology. All Rights Reserved.

Address correspondence to Nannan Luan, gjlkdd@163.com.

Received 7 February 2021

Returned for modification 21 February 2021

Accepted 24 April 2021

Accepted manuscript posted online 24 May 2021

Published 23 July 2021

their target genes, i.e., mRNAs, thereby upregulating or decreasing the expression of mRNAs (12, 13). For example, lncRNA XLOC_006390 acts as a ceRNA to positively regulate the expression of mRNA neuropilin 2 (NRP2)/pyruvate kinase M1/2 (PKM2) and eyes absent homolog 2 (EYA2) by interacting with miRNA 331-3p (miR-331-3p)/miR-338-3p, thereby promoting the tumorigenesis of CC (14). lncRNA syntaxin binding protein 5 (STXBP5) was reported to function as a ceRNA to decrease phosphatase and tensin homolog (PTEN) expression by binding with miR-96-5p, thus suppressing CC cell proliferation and invasion (15). Long intergenic non-protein-coding RNA 997 (LINC00997) is a newly identified molecule, which has 472 nucleotides in length from the start site, 32758881, to the end site, 32759353 (<http://www.noncode.org/index.php>). LINC00997 was discovered to promote cell metastasis in kidney renal clear cell carcinoma (16). LINC00997 was also reported to suppress the metastasis of colorectal cancer (17). In this study, we explored the functions and mechanism of LINC00997 in CC development. We hypothesized that LINC00997 may function as a ceRNA and affect cellular activities in CC.

Mitogen-activated protein kinase (MAPK) signaling pathways are involved in cellular processes such as cell growth, proliferation, migration, and apoptosis (18). Moreover, the role of MAPK signaling in CC progression has been verified. For example, lncRNA motor neuron and pancreas homeobox 1 antisense RNA 1 (MNX1-AS1) was reported to facilitate CC cell proliferation by activating MAPK signaling (19). lncRNA cancer susceptibility candidate 2 (CASC2) suppressed CC cell proliferation and invasion via inactivation of MAPK signaling (20). In this study, we hypothesized that LINC00997 might control the activation of MAPK signaling by modulating the expression of downstream genes, thus regulating cellular processes in CC.

This study focused on the role of LINC00997 in CC, which may provide new insight into molecular investigation in CC.

RESULTS

LINC00997 exhibits high expression in CC tissues and cells. We identified 10 lncRNAs (ADAMTS9-AS1, PGM5-AS1, RNF185-AS1, DLGAP1-AS1, LINC00997, ZSCAN16-AS1, FLVCR1-AS1, PRR34-AS1, SH3PXD2A-AS1, and RNF139-AS1) for our study. First, reverse transcription-quantitative PCR (RT-qPCR) was conducted to examine the expression levels of these lncRNAs in 58 paired CC tissues and adjacent normal tissues. The results showed that only LINC00997 exhibited significant high expression in CC tissues (Fig. 1A). Next, we examined LINC00997 expression in a normal cervical epithelial cell line and four CC cell lines. RT-qPCR revealed that LINC00997 expression was markedly increased in CC cell lines compared with that in the cervical epithelial cell line. Additionally, the most significant high expression of LINC00997 was detected in HeLa and SiHa cells; thus, the two cell lines were utilized for subsequent functional assays (Fig. 1B). Afterwards, the genomic copy number of LINC00997 was examined in 58 tumor tissues and 58 normal tissues utilizing RT-qPCR. The results showed that the genomic copy number of LINC00997 was also markedly increased in CC tissues compared with that in normal tissues (Fig. 1C). According to Pearson correlation analysis, the RNA expression level of LINC00997 was positively correlated with the genomic copy number of LINC00997 (Fig. 1D). The data indicated that the amplification of LINC00997 copy number partly resulted in the high expression of LINC00997 in CC. Overall, these findings verified that LINC00997 expression is upregulated in CC tissues and cells.

LINC00997 depletion inhibits CC cell proliferation, migration, invasion, and autophagy. Subsequently, we investigated the effect of LINC00997 on CC cellular processes. First, we knocked down LINC00997 expression with sh-LINC00997#1/2 in HeLa and SiHa cells (Fig. 2A). We identified sh-LINC00997#1 to conduct the following loss-of-function assays due to the better knockdown efficiency of sh-LINC00997#1 in HeLa and SiHa cells. The 3-(4,5-dimethyl-2-thiazolyl)-2,5-diphenyl-2H-tetrazolium bromide (MTT) assay was conducted to examine the effect of LINC00997 on CC cell viability; the results showed that the number of viable CC cells was reduced by LINC00997 knockdown (Fig. 2B). In addition, the number of cell colonies was decreased in HeLa

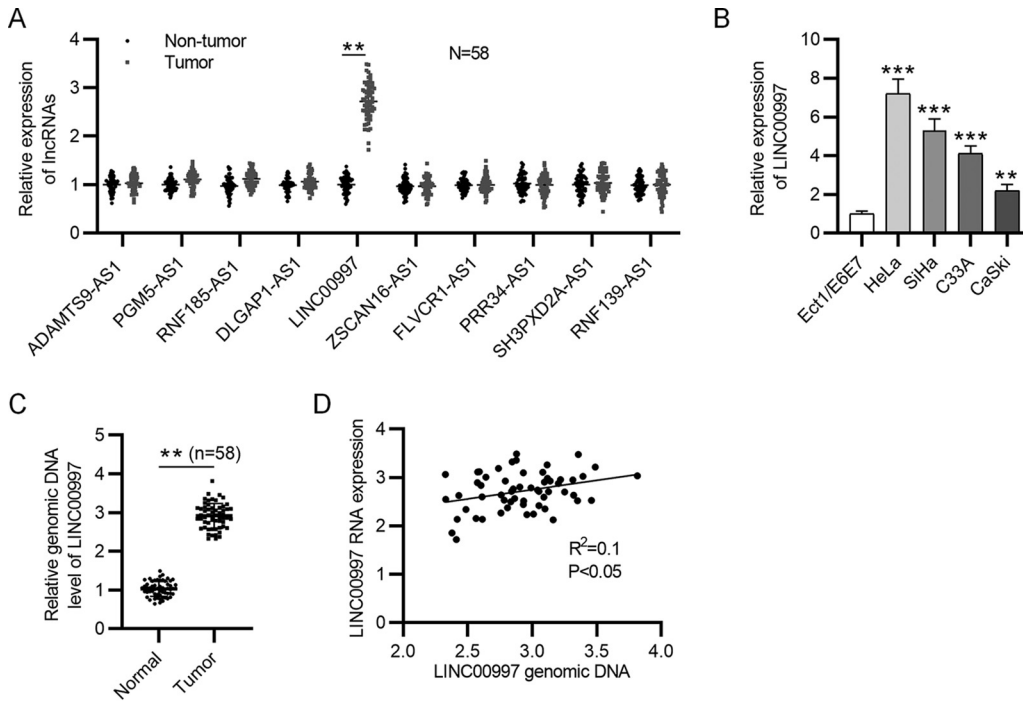


FIG 1 LINC00997 exhibits high expression in CC tissues and cells. (A) The expression levels of 10 lncRNAs in CC tissues and adjacent nontumor tissues were examined by RT-qPCR. Only LINC00997 showed significantly high expression in CC tissues. (B) RT-qPCR was conducted to detect LINC00997 expression in four CC cell lines and a cervical epithelial cell line (Ect1/E6E7). LINC00997 exhibited high expression in CC cell lines, especially in the HeLa and SiHa cell lines. (C) The genomic copy number of LINC00997 was examined by RT-qPCR in tumor tissues and normal tissues. (D) Pearson correlation analysis was applied to identify the association between LINC00997 RNA level and LINC00997 copy number. A positive correlation between LINC00997 RNA level and LINC00997 copy number was identified. **, $P < 0.01$; ***, $P < 0.001$.

and SiHa cells with transfection of sh-LINC00997#1, indicating that LINC00997 silencing reduced CC cell proliferation (Fig. 2C). Furthermore, Transwell assays revealed that LINC00997 depletion decreased the number of migrated and invaded cells, suggesting that the migratory and invasive capacities of CC cells were suppressed by LINC00997 knockdown (Fig. 2D and E). Upon transmission electron microscopy (TEM) observation, we discovered that the number of autophagosomes was reduced by LINC00997 depletion, suggesting that LINC00997 knockdown suppressed CC cell autophagy (Fig. 2F). In addition, as suggested by Western blot analysis, the ratio of LC3-II/LC3-I and beclin-1 protein levels was decreased by LINC00997 knockdown (Fig. 2G). Overall, LINC00997 depletion inhibits CC cell proliferation, migration, invasion, and autophagy.

LINC00997 interacts with miR-574-3p in CC. Afterwards, we explored the mechanism mediated by LINC00997 in CC. Mounting evidence suggests that cytoplasmic lncRNAs can act as ceRNAs in cancers (21, 22). According to the subcellular fractionation, LINC00997 was confirmed to be mainly distributed in the cytoplasm of CC cells (Fig. 3A), indicating that LINC00997 functions posttranscriptionally in CC. Next, we explored downstream genes of LINC00997. Fourteen potential LINC00997-binding miRNAs (miR-27a-3p, miR-27b-3p, miR-512-3p, miR-574-3p, miR-22-3p, miR-1301-3p, miR-126-5p, miR-485-3p, miR-101-3p, miR-221-3p, miR-222-3p, miR-134-5p, miR-26a-5p, and miR-26b-5p) were predicted from starBase (Fig. 3B). RNA pull-down assays were carried out to examine the interaction between LINC00997 and candidate miRNAs, and the results revealed that 3 miRNAs (miR-574-3p, miR-126-5p, and miR-101-3p) were significantly pulled down by LINC00997 biotinylated probes in HeLa cells. RNA pull-down assays were then performed in SiHa cells to determine the enrichment of the 3 miRNAs, and the results suggested that only miR-574-3p was highly enriched in LINC00997 biotinylated probes in SiHa cells (Fig. 3C). Thus, we identified miR-574-3p for further study. RT-qPCR indicated that miR-574-3p exhibited low expression in CC

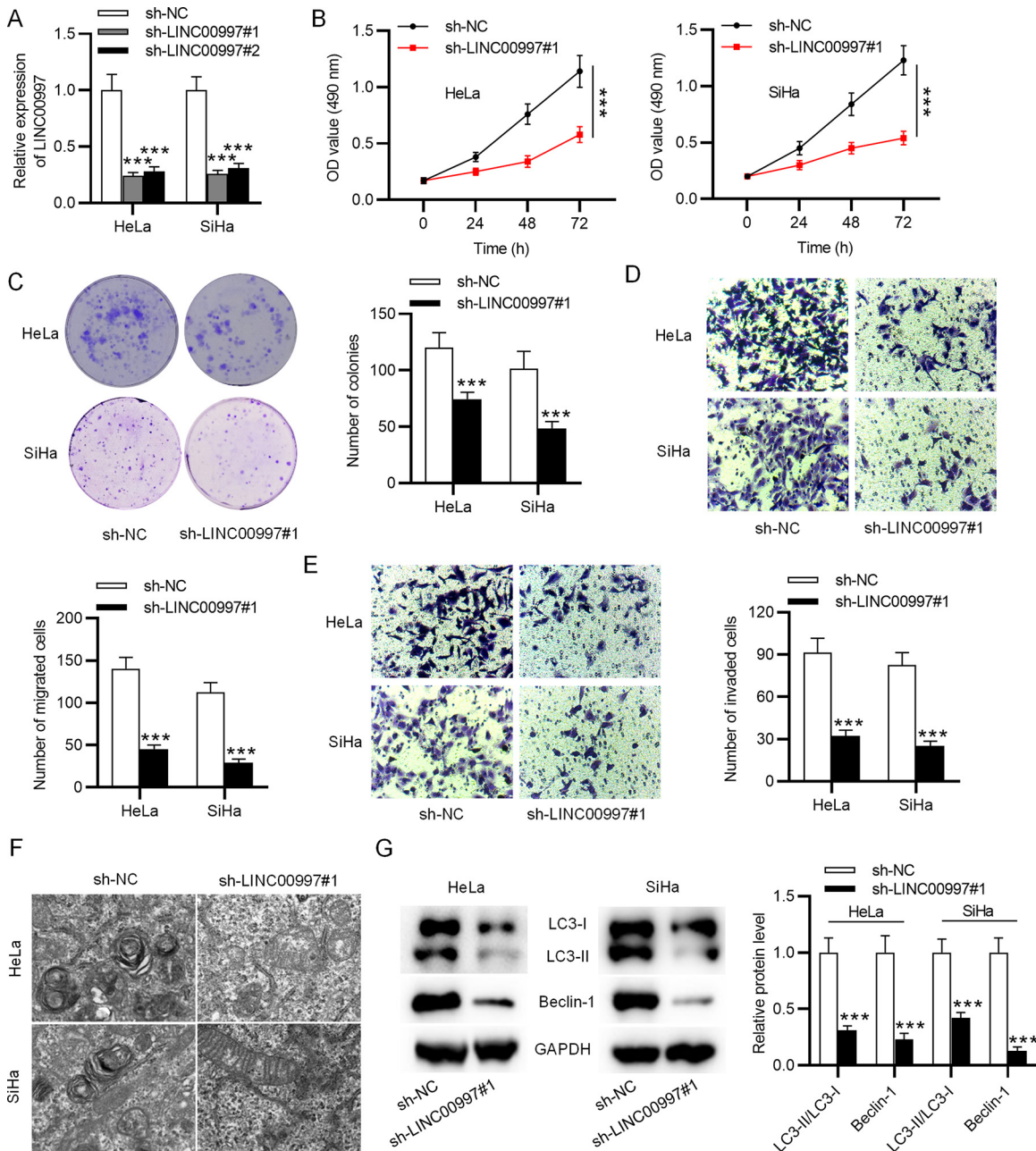


FIG 2 LINC00997 depletion inhibits CC cell proliferation, migration, invasion, and autophagy. (A) The knockdown efficiency of LINC00997 in HeLa and SiHa cells was detected by RT-qPCR. LINC00997 expression was markedly decreased especially in cells transfected with sh-LINC00997#1. (B and C) The viability and proliferation of HeLa and SiHa cells with transfection of sh-LINC00997#1 were assessed by MTT and colony formation assays. MTT and colony formation assays were repeated in triplicate. (D and E) The effect of LINC00997 deficiency on CC cell migration and invasion was evaluated by Transwell assays. All experiments were conducted thrice. (F) The number of autophagosomes after transfection of sh-LINC00997#1 was observed by TEM. TEM observation was performed three times. (G) The protein levels of autophagy markers (LC3-II/LC3-I and beclin-1) in CC cells with transfection of sh-LINC00997#1 were detected by Western blotting. ***, $P < 0.001$.

tissues and cells compared with that in nontumor tissues and cervical epithelial cells (Fig. 3D). Moreover, the genomic copy number of miR-574-3p was also downregulated in CC tissues compared with that in normal tissues (Fig. 3D). miR-574-3p expression was upregulated due to LINC00997 silencing in HeLa and SiHa cells (Fig. 3E). The over-expression efficiency of miR-574-3p mimics was examined by RT-qPCR (Fig. 3F). miR-574-3p overexpression failed to significantly affect LINC00997 expression in CC cells, as

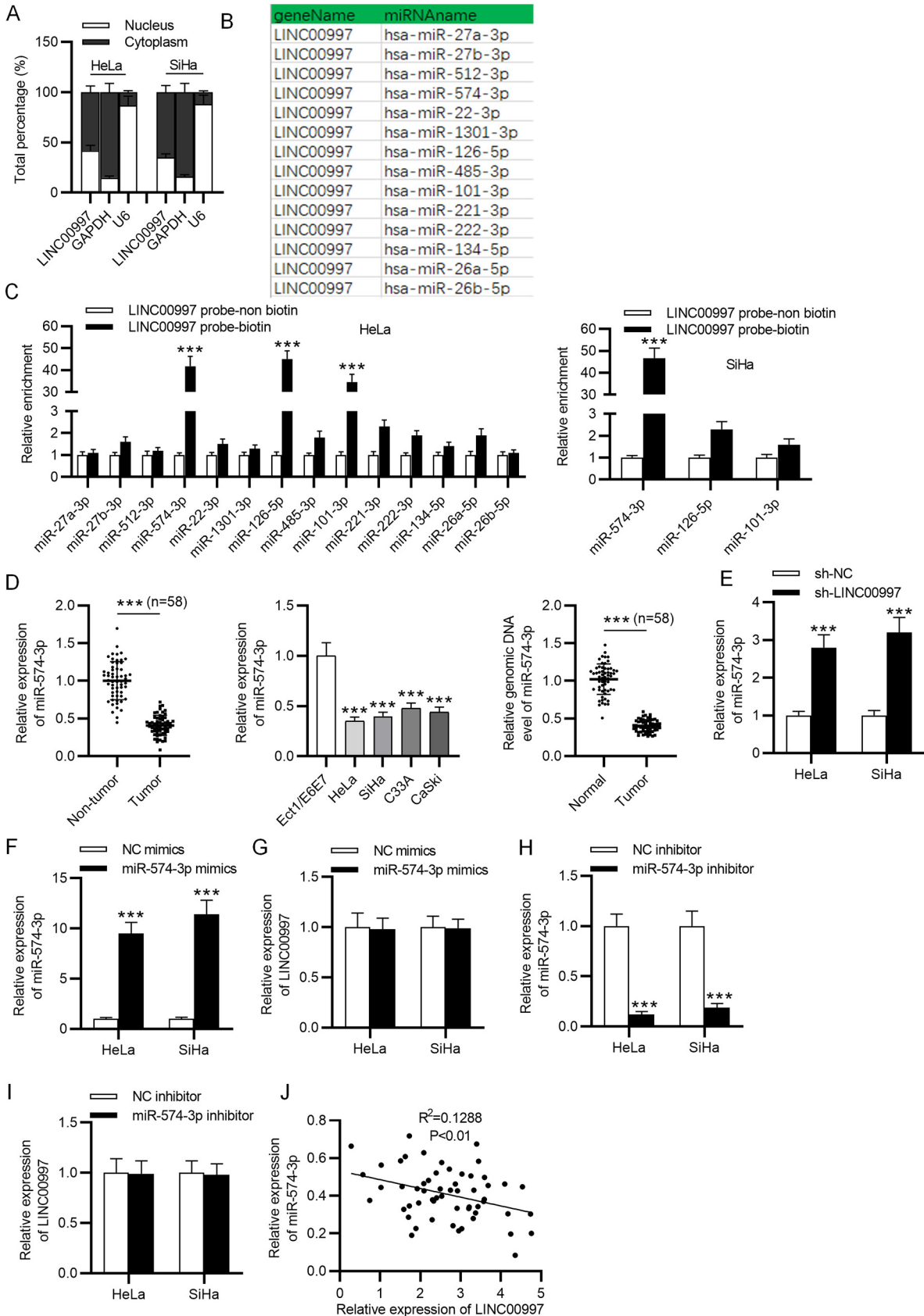


FIG 3 LINC00997 interacts with miR-574-3p in CC. (A) The distribution of LINC00997 in CC cells was determined by the subcellular fractionation assay. The assay was repeated thrice. (B) The 14 possible LINC00997-binding miRNAs were predicted from the starBase (Continued on next page)

suggested by RT-qPCR (Fig. 3G). The efficiency of miR-574-3p silencing in HeLa and SiHa cells was detected by RT-qPCR (Fig. 3H). Similarly, inhibition of miR-574-3p failed to change LINC00997 expression in CC cells (Fig. 3I). In addition, Pearson correlation analysis identified the negative expression correlation between LINC00997 expression and miR-574-3p expression in CC tissues (Fig. 3J). In summary, LINC00997 interacts with miR-574-3p in CC.

CUL2 is targeted by miR-574-3p in CC. Next, we explored the target gene of miR-574-3p in CC utilizing databases (microT, PITA, and PicTar) on the starBase website. As illustrated by the Venn diagram in Fig. 4A, 2 mRNAs, cullin 2 (CUL2) and striatin 2 (STRN3), were predicted by the microT, PITA, and PicTar databases. Next, RT-qPCR was conducted to examine the effect of miR-574-3p overexpression on the expression of two candidate target genes in CC cells. After miR-574-3p overexpression, CUL2 expression in HeLa and SiHa cells was significantly downregulated, while STRN3 expression exhibited no significant changes (Fig. 4B). Thus, we identified CUL2 for further study. A possible binding site between miR-574-3p and the 3' untranslated region (UTR) of CUL2 was predicted from starBase, and the CUL2 sequence was mutated (Fig. 4C). According to a luciferase reporter assay, the luciferase activities of CUL2-Wt reporters were impaired by miR-574-3p mimics, while those of CUL2-Mut reporters exhibited no significant changes (Fig. 4C). The results implied the direct binding between miR-574-3p and the 3' UTR of CUL2. In another luciferase reporter assay, we mutated the sequence of miR-574-3p and discovered that the luciferase activity of CUL2 was increased by LINC00997 overexpression in the miR-574-3p-Wt group, with no significant changes detected in the miR-574-3p-Mut group (Fig. 4D). The results suggested that LINC00997 upregulated CUL2 expression by competitively interacting with miR-574-3p. Next, we inhibited miR-574-3p expression with miR-574-3p inhibitor in HeLa and SiHa cells for RNA-binding protein immunoprecipitation (RIP) assays. As shown in RT-qPCR, miR-574-3p expression was markedly decreased (Fig. 4E). RIP assays were performed to further explore the relationship of the three factors. LINC00997 was significantly enriched in Ago2 antibody after miR-574-3p overexpression (Fig. 4F). Similarly, the enrichment of CUL2 mRNA in Ago2 antibody was increased by miR-574-3p overexpression compared with that in the anti-IgG group (Fig. 4G). The enrichment of LINC00997 and CUL2 mRNA in the antibody Ago2 group was decreased due to miR-574-3p inhibition (Fig. 4H and I). Overall, CUL2 is a target gene of miR-574-3p, and LINC00997 upregulates CUL2 expression via miR-574-3p in CC.

LINC00997 positively regulates mRNA expression and protein level of CUL2 by binding to miR-574-3p. RT-qPCR revealed that CUL2 exhibited high expression in CC tissues and cells compared with its expression in nontumor tissues and cervical epithelial cells (Fig. 5A and B). The genomic copy number of CUL2 in tissues was examined by RT-qPCR, and the results implied that the CUL2 genomic DNA level was also increased in CC tissues compared with that in normal tissues (Fig. 5C). Pearson correlation analysis suggested that CUL2 expression was negatively associated with miR-574-3p expression and positively correlated with LINC00997 expression in CC tissues (Fig. 5D and E). RT-qPCR and Western blot analyses were performed to explore the effect of LINC00997 silencing and miR-574-3p inhibition on CUL2 levels in CC cells. Both mRNA expression and protein level of CUL2 were markedly increased due to miR-574-3p inhi-

FIG 3 Legend (Continued)

website under the condition of Pan-Cancer, i.e., 4 cancer types. (C) RNA pulldown assays were conducted to detect the enrichment of candidate miRNAs in LINC00997 biotin probes, and they were performed in triplicate. (D) miR-574-3p expression in CC tissues and cells and miR-574-3p copy number in CC tissues were examined by RT-qPCR. miR-574-3p expression was decreased in CC tissues and cells compared with that in control groups, and miR-574-3p copy number was also decreased in tumor tissues. (E) The effect of LINC00997 knockdown on miR-574-3p expression was examined by RT-qPCR. miR-574-3p expression was upregulated due to LINC00997 silencing in HeLa and SiHa cells. (F) The efficiency of miR-574-3p overexpression in CC cells was probed by RT-qPCR. miR-574-3p expression was successfully increased by miR-574-3p mimics. (G) The effect of miR-574-3p overexpression on LINC00997 expression was examined by RT-qPCR. No significant changes were examined in LINC00997 expression after miR-574-3p overexpression. (H) RT-qPCR was performed to detect the efficiency of miR-574-3p inhibition in CC cells. (I) RT-qPCR was conducted to explore whether the inhibition of miR-574-3p might regulate LINC00997 expression. miR-574-3p silencing failed to affect LINC00997 expression in CC cells. (J) LINC00997 expression was negatively associated with miR-574-3p expression in CC tissues as identified by Pearson correlation analysis. ***, $P < 0.001$.

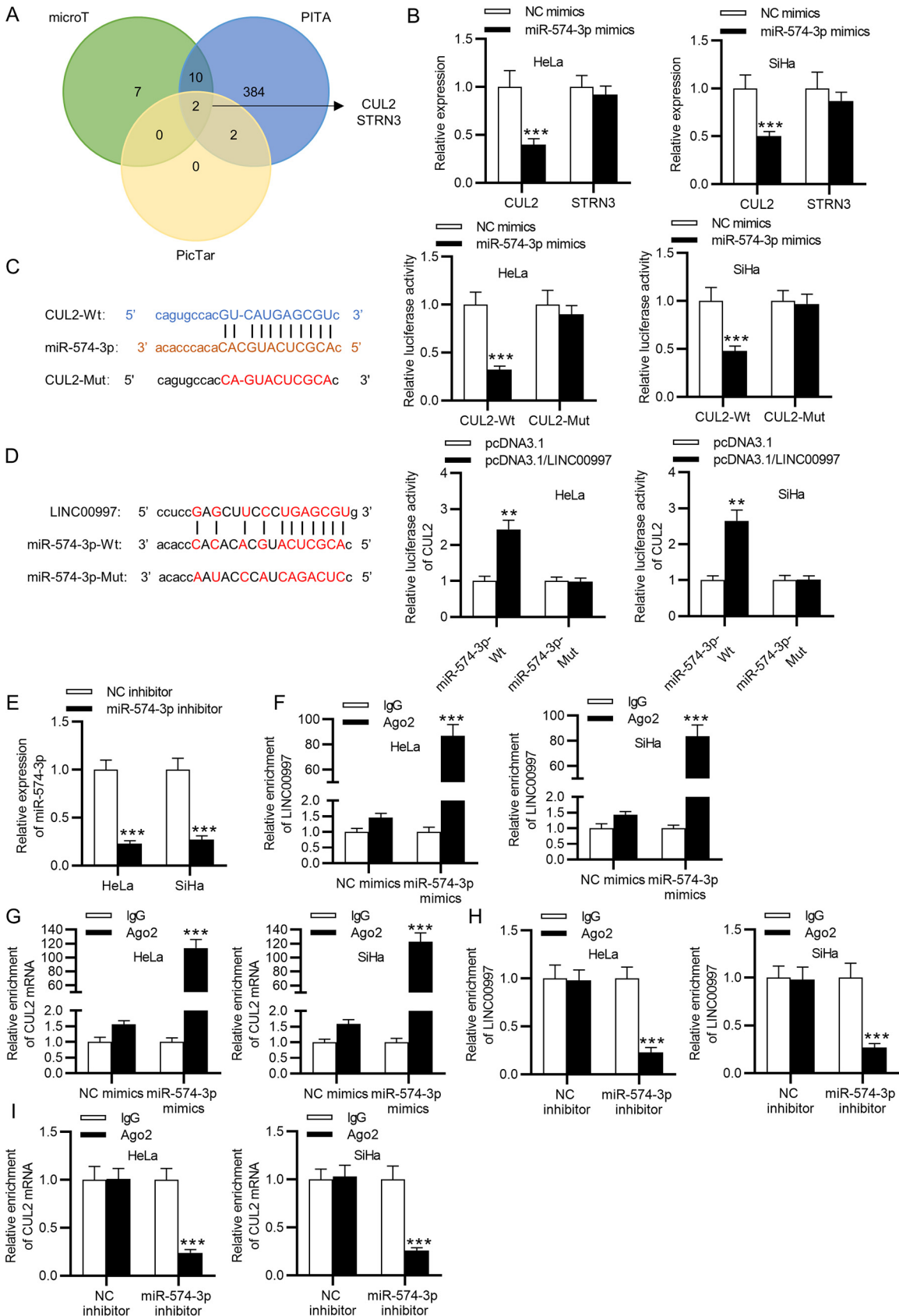


FIG 4 CUL2 is targeted by miR-574-3p. (A) Two miR-574-3p-binding mRNAs (CUL2 and STRN3) were predicted from the starBase website. As illustrated by the Venn diagram, mRNA CUL2 and STRN3 were identified since they were simultaneously predicted by the (Continued on next page)

bition in HeLa and SiHa cells (Fig. 5F). The mRNA expression and protein level of CUL2 were downregulated by LINC00997 silencing, while the inhibition of miR-574-3p rescued the decrease in CUL2 levels (Fig. 5G). The results implied that miR-574-3p suppressed CUL2 levels at both the protein and mRNA levels, and LINC00997 positively regulated CUL2 levels by interacting with miR-574-3p.

CUL2 overexpression promotes malignant phenotypes of CC cells and activates the MAPK signaling pathway. We carried out a range of gain-of-function assays to explore the effect of CUL2 on CC cellular processes. As shown in RT-qPCR, both mRNA expression and protein level of CUL2 were markedly increased by pcDNA3.1/CUL2 in HeLa cells (Fig. 6A). MTT and colony formation assays suggested that CUL2 overexpression enhanced CC cell viability and proliferation (Fig. 6B and C). Moreover, cell migration and invasion were also promoted by pcDNA3.1/CUL2 (Fig. 6D and E). The number of autophagosomes was increased by CUL2 overexpression according to TEM observation, implying that CUL2 promoted the autophagy of CC cells (Fig. 6F). The ratio of LC3-II/LC3-I and beclin-1 protein levels was increased by pcDNA3.1/CUL2, which confirmed the promotion of autophagy by CUL2 overexpression (Fig. 6G). Furthermore, the phosphorylated extracellular signal-regulated kinase (ERK)/total ERK (p/t-ERK), p/t-c-Jun N-terminal protein kinase (p/t-JNK), and p/t-p38 protein ratios were increased by CUL2 overexpression, implying that the MAPK signaling was activated by CUL2 overexpression (Fig. 6H). Overall, CUL2 overexpression promotes cell proliferation, migration, invasion, and autophagy. In addition, CUL2 overexpression activates the MAPK signaling pathway.

CUL2 overexpression rescues the suppressive effect of LINC00997 knockdown on CC cell proliferation, migration, invasion, and autophagy. To confirm whether LINC00997 promotes malignant phenotypes of CC cells by upregulating CUL2 expression, rescue assays were carried out. As illustrated by MTT and colony formation assays, CUL2 overexpression rescued the inhibitory effect of LINC00997 knockdown on CC cell viability and proliferation (Fig. 7A and B). Transwell assays indicated that the suppressive effect of LINC00997 silencing on CC cell migration and invasion was reversed by CUL2 overexpression (Fig. 7C). Moreover, CUL2 overexpression rescued the decrease in the number of autophagosomes caused by LINC00997 depletion in HeLa cells (Fig. 7D). Additionally, the inhibitory effect on the ratio of LC3-II/LC3-I and beclin-1 protein levels mediated by LINC00997 silencing was also reversed by CUL2 overexpression (Fig. 7E). The results suggested that CUL2 rescued the suppressive effect on autophagy mediated by LINC00997 in CC cells. In summary, rescue assays demonstrated that LINC00997 promotes CC cell proliferation, migration, invasion, and autophagy by upregulating CUL2 expression.

CUL2 overexpression rescues the inhibitory effect of miR-574-3p overexpression on malignant phenotypes of CC cells. To explore the effect of miR-574-3p on cellular processes and its mechanistic relationship with CUL2, gain-of-function experiments were carried out. MTT and colony formation assays revealed that miR-574-3p overexpression suppressed CC cell viability and proliferation, while CUL2 overexpression rescued the suppressive effect (Fig. 8A and B). Transwell assays suggested that CUL2 overexpression reversed the inhibitory effect of miR-574-3p overexpression on cell migration and invasion (Fig. 8C). As determined by TEM observation, miR-574-3p over-

FIG 4 Legend (Continued)

microT, PITA, and PicTar databases. (B) The effect of miR-574-3p overexpression on mRNA levels of CUL2 and STRN3 in CC cells was evaluated by RT-qPCR. CUL2 expression was downregulated by miR-574-3p mimics, while STRN3 expression exhibited no significant changes compared with the control group in CC cells. (C) The binding site between CUL2 and miR-574-3p was predicted from starBase, and the CUL2 3' UTR fragment was mutated. The luciferase assay was applied to explore the interaction between miR-574-3p and CUL2. (D) The binding site between LINC00997 and miR-574-3p was also predicted from starBase, and the miR-574-3p sequence was mutated. The luciferase activities of CUL2 was examined in CC cells overexpressing LINC00997 with or without the miR-574-3p binding site being mutated. (E) miR-574-3p expression was silenced by the miR-574-3p inhibitor, and the efficiency of miR-574-3p inhibition was detected by RT-qPCR. (F and G) RIP assay was conducted to examine the enrichment of LINC00997 and CUL2 mRNA in the Ago2 group or IgG group in CC cells transfected with miR-574-3p mimics. LINC00997 and CUL2 mRNA were markedly enriched in Ago2 antibody group after miR-574-3p overexpression. (H and I) The enrichment of LINC00997 and CUL2 mRNA in the Ago2 group or IgG group was decreased due to the inhibition of miR-574-3p, as suggested by RIP assays. All experiments were performed three times. **, $P < 0.01$; ***, $P < 0.001$.

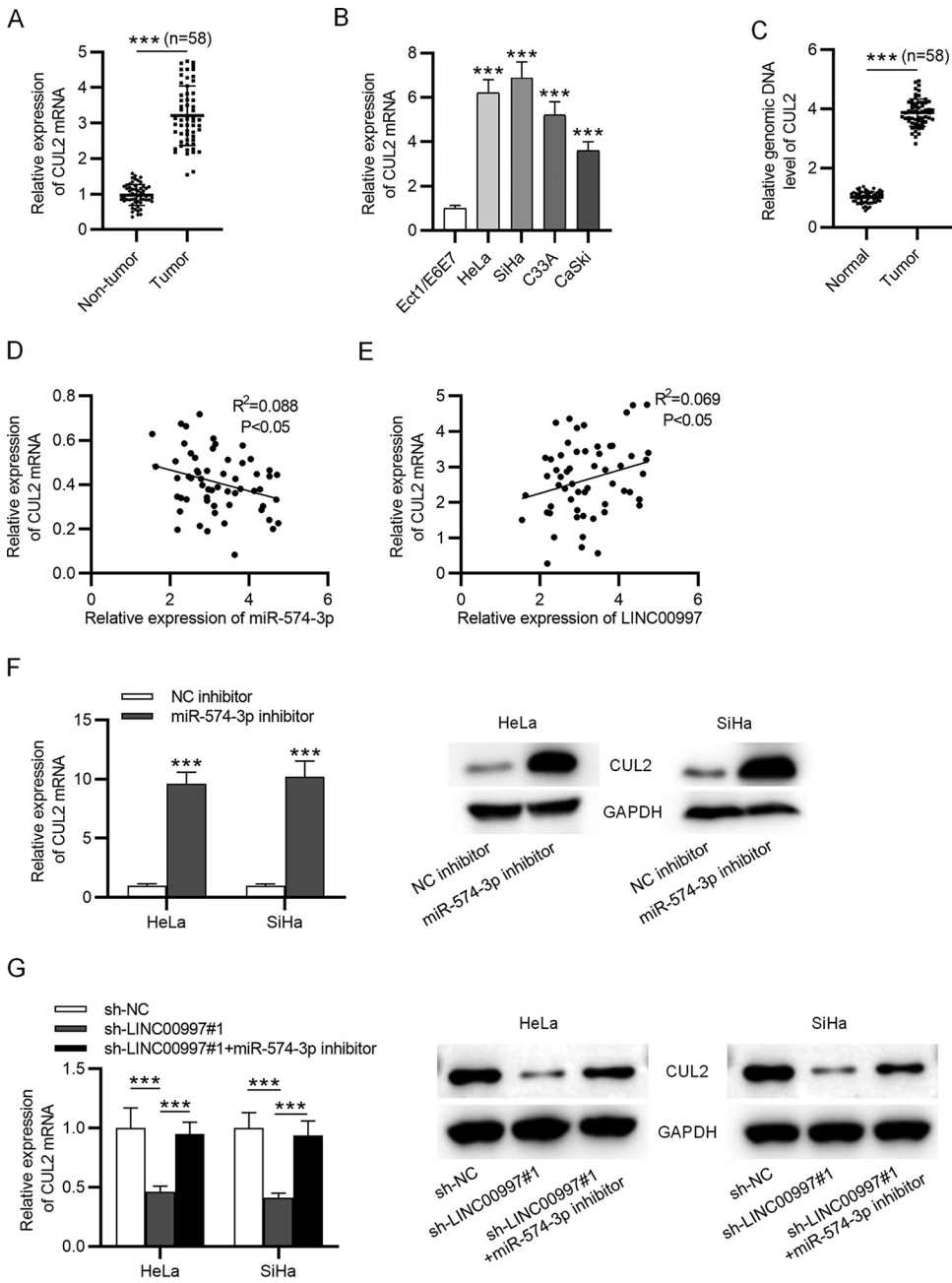


FIG 5 LINC00997 upregulates mRNA expression and protein level of CUL2 by binding to miR-574-3p. (A and B) The expression of CUL2 in CC tissues and cells was probed by RT-qPCR. CUL2 is highly expressed in CC tissues and cells compared with nontumor tissues and epithelial cells. (C) The genomic copy number of CUL2 was also increased in 58 CC tissues compared with that in 58 normal tissues, as suggested by RT-qPCR. (D and E) CUL2 expression was negatively correlated with miR-574-3p expression and positively associated with LINC00997 expression in CC tissues, as identified by Pearson correlation analysis. (F) The mRNA expression and protein level of CUL2 were increased due to miR-574-3p inhibition, as suggested by RT-qPCR and Western blot analyses. (G) Inhibition of miR-574-3p rescued the decrease in mRNA expression and protein level of CUL2 induced by LINC00997 silencing according to RT-qPCR and Western blotting. ***, $P < 0.001$.

expression inhibited cell autophagy, while CUL2 overexpression rescued the inhibitory effect (Fig. 8D). Similarly, CUL2 overexpression successfully reversed the decrease in protein levels of autophagy markers in HeLa cells (Fig. 8E). In conclusion, CUL2 overexpression rescued the inhibitory effect on cell proliferation, migration, invasion, and autophagy mediated by miR-574-3p overexpression.

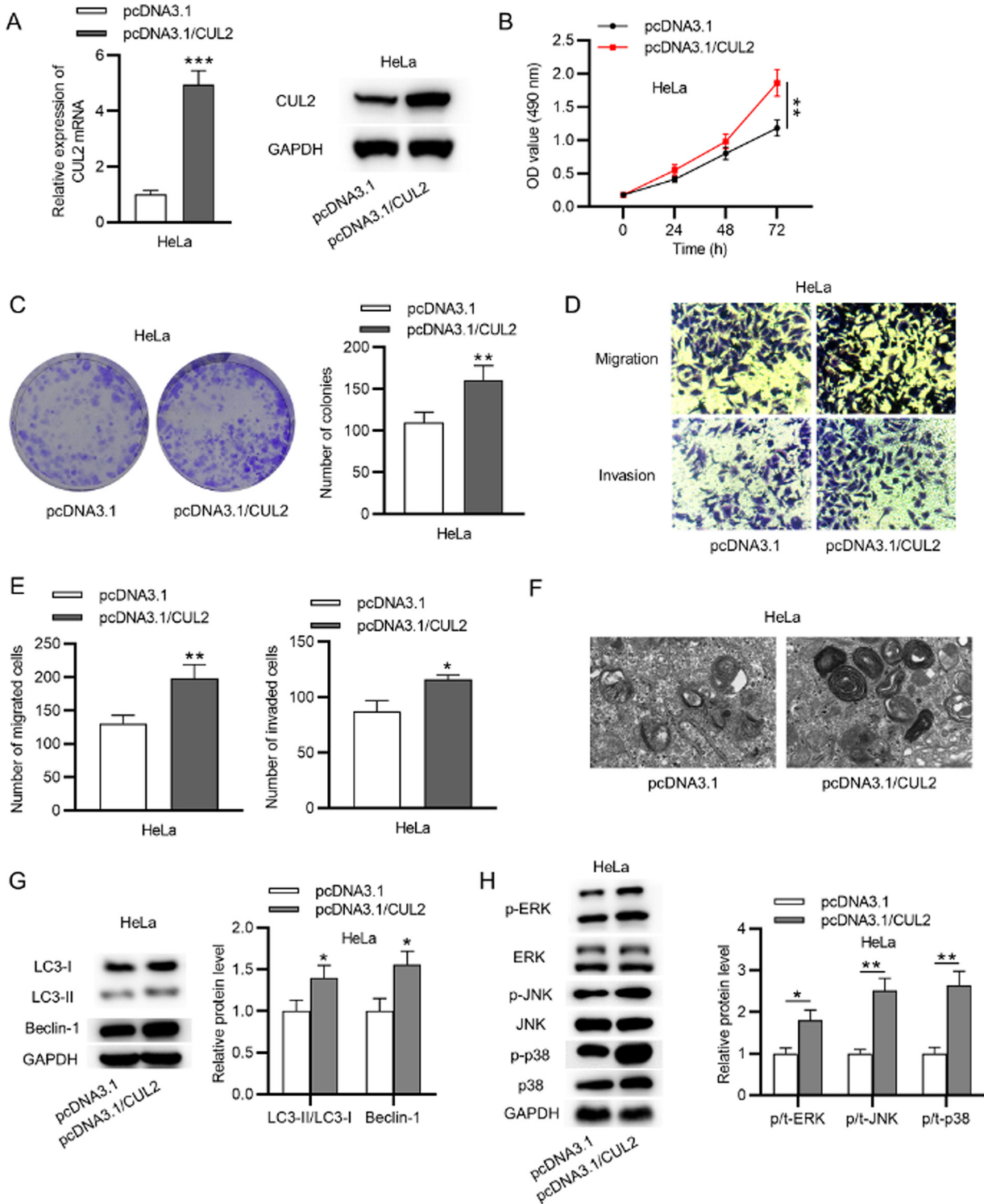


FIG 6 CUL2 overexpression promotes malignant phenotypes of CC cells and activates MAPK signaling. (A) RT-qPCR and Western blot analyses were performed to examine the overexpression efficiency of CUL2 in HeLa cells. (B and C) CC cell viability and proliferation were enhanced by CUL2 overexpression as shown in MTT and colony formation assays. All experiments were repeated in triplicate. (D and E) The migratory and invasive capacities of CC cells were promoted by pcDNA3.1/CUL2 according to Transwell assays. All assays were performed three times. (F) TEM observation was utilized to probe the effect of CUL2 overexpression on the number of autophagosomes. The experiment was conducted three times. (G) Western blot analysis was employed to detect protein levels of autophagy markers in HeLa cells transfected with pcDNA3.1/CUL2. (H) The levels of proteins related to the MAPK signaling pathway were examined by Western blot analysis. *, $P < 0.05$; **, $P < 0.01$; ***, $P < 0.001$.

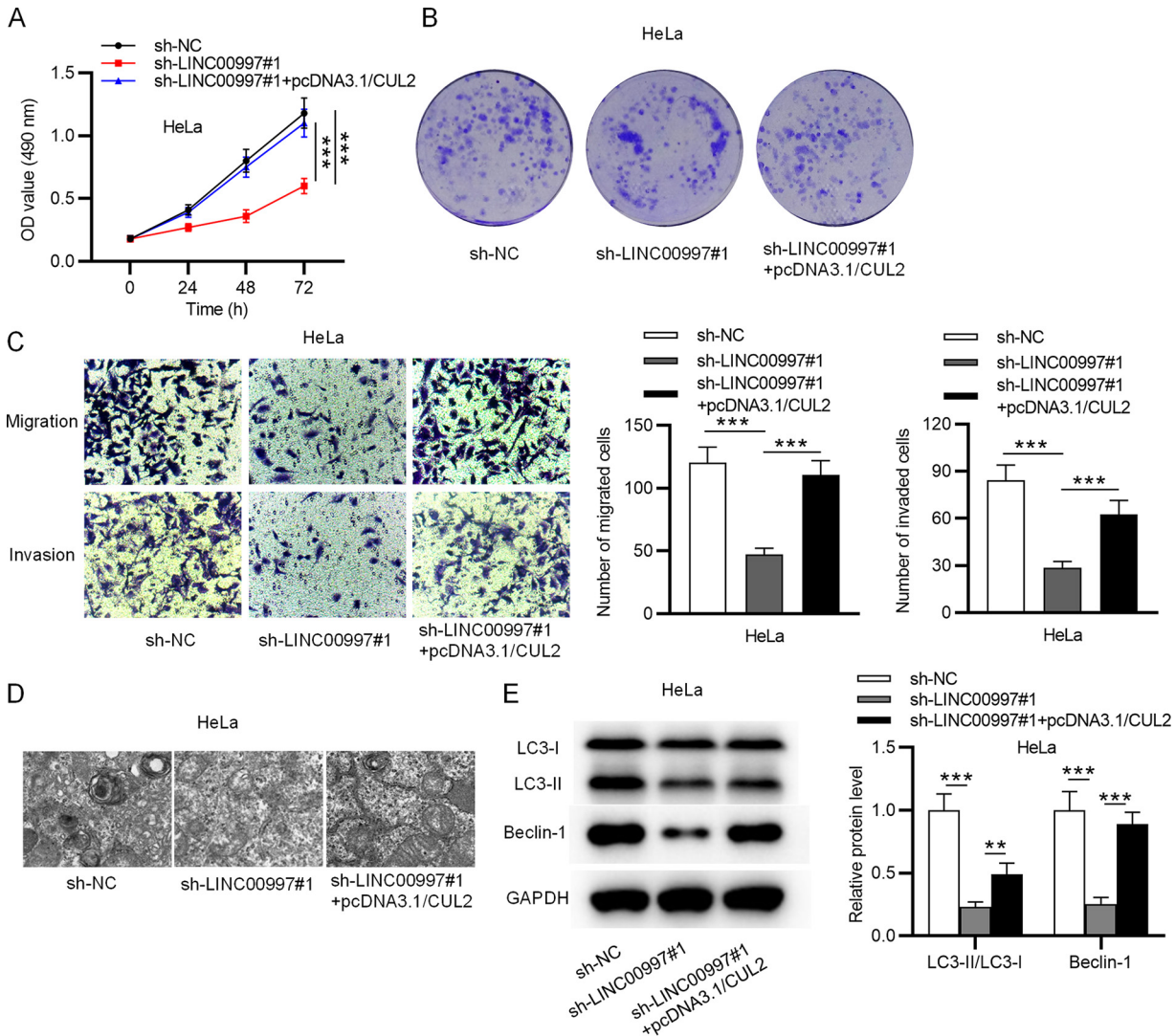


FIG 7 LINC00997 promotes CC cell proliferation, migration, invasion, and autophagy by upregulating CUL2 expression. (A and B) MTT and colony formation assays were conducted to evaluate the viability and proliferation of CC cells transfected with sh-NC or sh-LINC00997#1 and/or pcDNA3.1/CUL2. All experiments were repeated thrice. (C) Transwell assays were employed to measure CC cell migration and invasion after transfection. All experiments were performed in triplicate. (D) TEM was applied to observe effects of LINC00997 knockdown and/or CUL2 overexpression on the number of autophagosomes and was performed three times. (E) The ratio of LC3-II/LC3-I and beclin-1 protein level in CC cells with transfection was examined by Western blot analysis. *, $P < 0.05$; **, $P < 0.01$; ***, $P < 0.001$.

LINC00997 activates the MAPK signaling by upregulating CUL2 expression. Since CUL2 can activate the MAPK signaling and CUL2 was positively regulated by LINC00997 in CC, we investigated whether LINC00997 can affect activation of MAPK signaling by regulating CUL2 expression. As delineated by Western blot analysis, CUL2 overexpression reversed the decrease in protein levels of p-ERK, p-JNK, and p-p38 in HeLa cells mediated by LINC00997 knockdown (Fig. 9A). For further exploration, we overexpressed LINC00997 and silenced CUL2 expression in SiHa cells (Fig. 9B). Western blot analysis revealed that CUL2 knockdown reversed the increase in protein levels of p-ERK, p-JNK, and p-p38 mediated by LINC00997 overexpression (Fig. 9C). Thus, we concluded that LINC00997 activates MAPK signaling via the upregulation of CUL2 expression.

DISCUSSION

In recent decades, the biological functions of lncRNAs have been widely investigated (23, 24). Additionally, dysregulated lncRNAs are acknowledged as key factors in

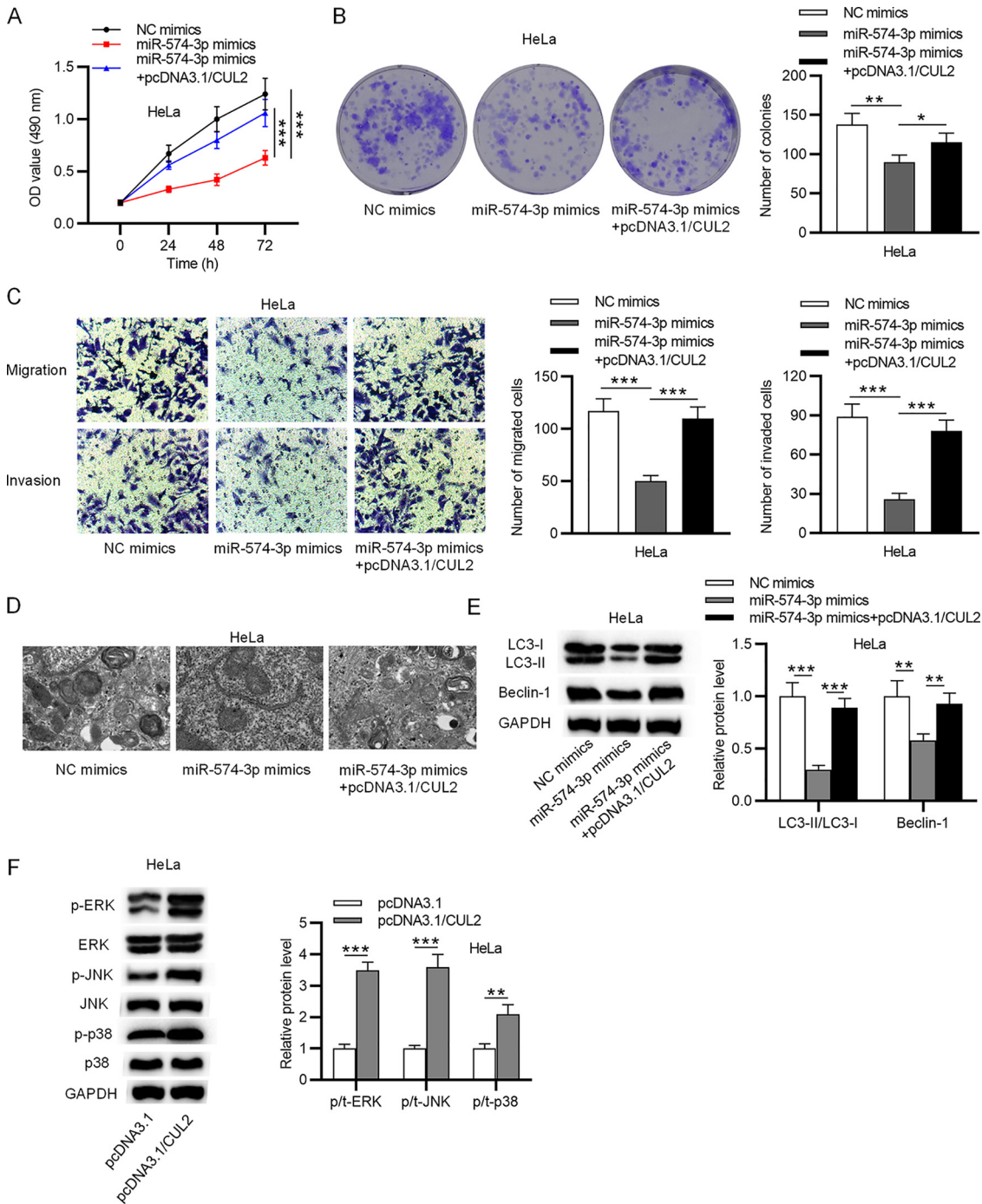


FIG 8 CUL2 overexpression rescues the suppressive effect of miR-574-3p overexpression on malignant phenotypes of CC cells. (A and B) The viability and proliferation of CC cells transfected with miR-574-3p mimics, NC mimics, or miR-574-3p mimics+pcDNA3.1/CUL2 were probed by MTT and colony formation assays. (C) Cell migration and invasion were inhibited by miR-574-3p overexpression and rescued by CUL2 overexpression according to Transwell assays. (D) The autophagy of HeLa cells after transfection was probed by TEM observation. (E) The protein levels of LC3-II/LC3-I and beclin-1 in HeLa cells with transfection were examined by Western blot analysis. (F) The effect of CUL2 overexpression on protein levels of MAPK pathway-associated factors was detected by Western blot analysis. *, $P < 0.05$; **, $P < 0.01$; ***, $P < 0.001$.

the tumorigenesis of cancers (25, 26). Our study showed that LINC00997 expression was upregulated in CC tissues and cells. In addition, LINC00997 copy number was also increased in CC tissues. LINC00997 RNA expression positively correlated with LINC00997 copy number, implying that LINC00997 copy number partly resulted in the

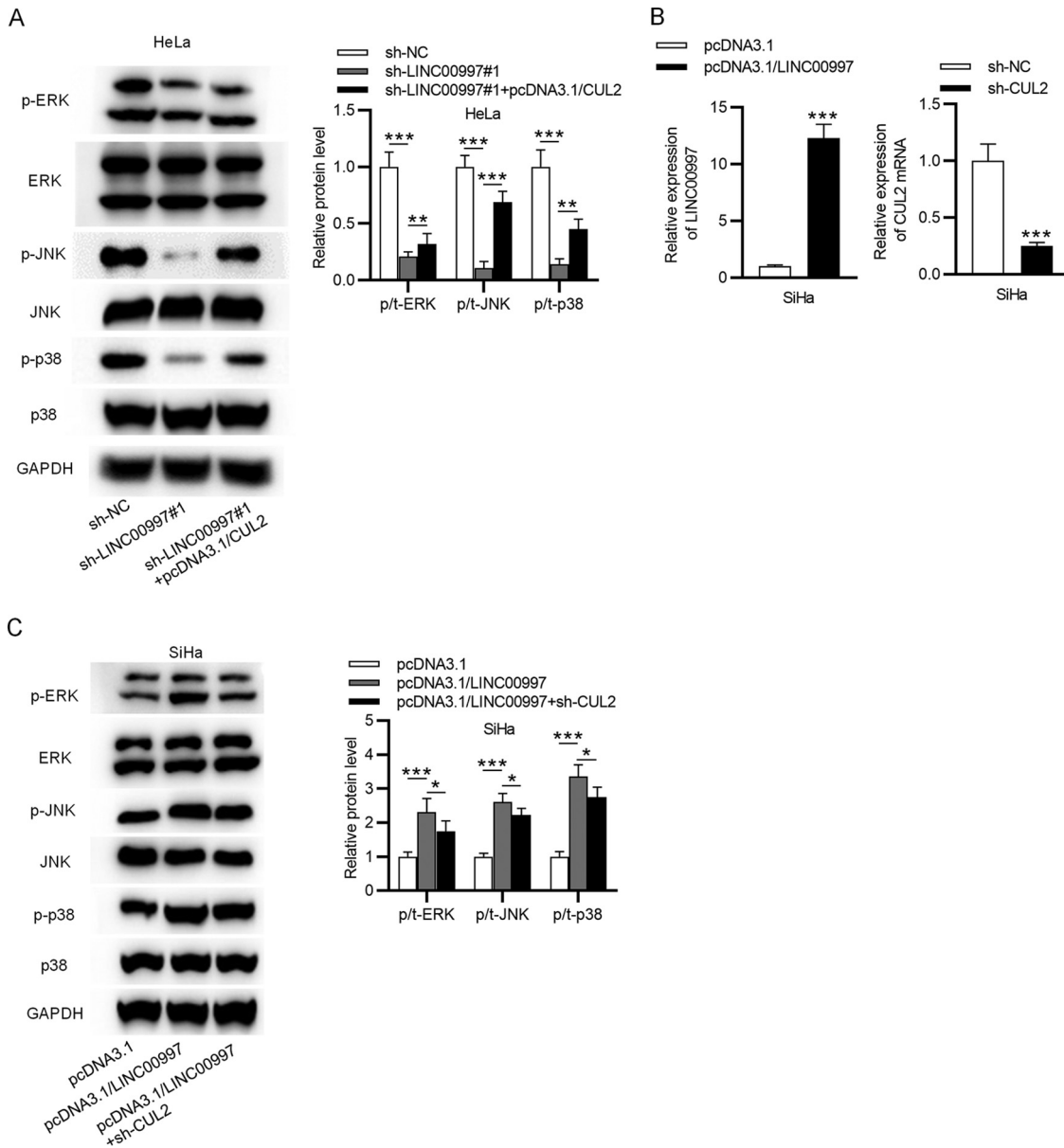


FIG 9 LINC00997 activates MAPK signaling by upregulating CUL2 expression. (A) Western blot analysis was carried out to probe effects of LINC00997 knockdown and/or CUL2 overexpression on protein levels of MAPK pathway-related factors in HeLa cells. CUL2 overexpression reversed the decrease in protein levels of p-ERK, p-JNK, and p-p38 in HeLa cells mediated by LINC00997 knockdown. (B) The efficiency of LINC00997 overexpression or CUL2 knockdown in SiHa cells was measured by RT-qPCR. (C) The protein levels of phosphorylated ERK/JNK/P38 in SiHa cells with transfection of pcDNA3.1, pcDNA3.1/LINC00997, or pcDNA3.1/LINC00997+sh-CUL2 were measured by Western blot analysis. CUL2 knockdown reversed the increase in protein levels of p-ERK, p-JNK, and p-p38 mediated by LINC00997 overexpression. *, $P < 0.05$; **, $P < 0.01$; ***, $P < 0.001$.

high expression of LINC00997 in CC. LINC00997 depletion suppressed CC cell proliferation, migration, and invasion. In addition, we discovered that LINC00997 knockdown inhibited the autophagy of CC cells. Autophagy refers to cellular material being transferred to lysosomes for degradation, resulting in the turnover of cell components and offering energy (27). Prevention or stimulation of autophagy is regarded as an effective theoretical option for cancer treatment (28). Thus, the oncogenic role of LINC00997 in CC development was confirmed.

Recent studies have shown that lncRNAs can serve as ceRNAs against miRNAs to play critical roles in cancer progression (13, 29). miRNAs are short noncoding RNAs of

approximately 22 nucleotides, which participate in posttranscriptional gene regulation and biological processes of many tumors (30). We discovered that LINC00997 is mainly localized in the cytoplasm of CC cells, suggesting that LINC00997 might function at the posttranscriptional level. Based on bioinformatics analyses and our experiments, we identified that LINC00997 bound to miR-574-3p in CC. According to a previous report, miR-574-3p represses the metastasis of epithelial ovarian cancer by targeting epidermal growth factor receptor (31). miR-574-3p represses colorectal cancer progression by directly binding to cyclin D2 (32). miR-574-3p attenuates cisplatin resistance by down-regulating zinc finger E-box binding homeobox transcription factor 1 in gastric carcinoma (33). In this study, miR-574-3p expression was decreased in CC tissues and cells, and its expression was negatively associated with LINC00997 expression or CUL2 expression in CC tissues. CUL2 is a target gene of miR-574-3p.

Under the control of the ceRNA network, miRNAs regulate gene expression posttranscriptionally by binding to the 3' UTRs of mRNAs (34). As suggested by previous studies, CUL2 upregulation promotes the occurrence of human papillomavirus 16 (HPV16) E7-induced CC (35). Moreover, CUL2 is related to a dismal prognosis for patients with esophageal cancer after neoadjuvant radiochemotherapy (36). Additionally, CUL2 can promote the tumorigenesis of colorectal cancer (37). In our study, CUL2 was found to exhibit high expression in CC tissues and cells. CUL2 expression was positively correlated with LINC00997 expression and negatively associated with miR-574-3p expression. In addition, miR-574-3p inhibition reversed the suppressive effect of LINC00997 silencing on mRNA expression and protein level of CUL2, suggesting that LINC00997 upregulated CUL2 expression by combining with miR-574-3p. CUL2 overexpression promoted malignant phenotypes of CC cells. In rescue assays, we validated that miR-574-3p suppressed CC cell proliferation, migration, invasion, and autophagy by decreasing CUL2 expression, while LINC00997 promoted malignant phenotypes of CC cells via the activation of MAPK signaling by upregulating CUL2 expression.

It has been recognized that lncRNAs can influence cancer occurrence and development via the MAPK pathway (38–40). To explore whether LINC00997 modulates MAPK signaling by regulating CUL2 expression, we examined the protein levels of factors (extracellular signal-regulated kinase [ERK], c-Jun N-terminal kinase [JNK], and p38) associated with the pathway. Previous evidence demonstrated that the deregulation of kinases such as ERK, JNK, and p38 can result in many human diseases, including cancer (41). The results indicated that CUL2 overexpression rescued the suppressive effect of LINC00997 knockdown on phosphorylated ERK, JNK, and p38 levels. Additionally, CUL2 silencing reversed the increase in phosphorylated ERK, JNK, and p38 protein levels induced by LINC00997 overexpression. Thus, we concluded that LINC00997 activated the MAPK pathway by increasing CUL2 expression via miR-574-3p.

In summary, the LINC00997/miR-574-3p/CUL2 axis promotes CC cell proliferation, migration, invasion, and autophagy by activating MAPK signaling. CUL2 is a target gene of miR-574-3p, and CUL2 expression is downregulated by miR-574-3p expression. LINC00997 serves as a ceRNA to combine with miR-574-3p, thereby preventing the degradation of CUL2. This study may provide new insight into molecular investigation in CC. However, animal experiments were not designed and the upstream signal of LINC00997 was not investigated in this study, which will be further explored in our future studies.

MATERIALS AND METHODS

Bioinformatics analysis. The 14 potential miRNAs binding to LINC00997 were predicted from the starBase website (<http://starbase.sysu.edu.cn/>) under the condition of Pan-Cancer, i.e., 4 cancer types (42). The mRNAs targeted by miR-574-3p were predicted from databases (microT, PITA, and PicTar) on the website of starBase. The results were illustrated by Venn diagram (<http://bioinformatics.psb.ugent.be/webtools/Venn/>) (43).

Tissue samples. CC tissues and adjacent noncancerous tissues were obtained from 58 CC patients at Shengjing Hospital of China Medical University (Liaoning, China). The collected tissues were stored at -80°C for experimental use. No patients had received preoperative anticancer treatment. All patients

TABLE 1 Primer sequences used for RT-qPCR

Target	Primer sequences
LINC00997	Forward, 5'-CCCTTAACCCACATACCAC-3'; reverse, 5'-TAGAATACTGGCATCGTTACAC-3'
miR-27a-3p	Forward, 5'-TTCACAGTGGCTAAGTTCCG-3'; reverse, 5'-CTCTACAGCTATATTGCCAGCC-3'
miR-27b-3p	Forward, 5'-TTCACAGTGGCTAAGTTCTGC-3'; reverse, 5'-CTCTACAGCTATATTGCCAGCC-3'
miR-512-3p	Forward, 5'-AAGTGTGTCATAGCTGAGGTC-3'; reverse, 5'-CTCTACAGCTATATTGCCAGCC-3'
miR-574-3p	Forward, 5'-CACGCTCATGCACACACC-3'; reverse, 5'-CTCTACAGCTATATTGCCAGCC-3'
miR-22-3p	Forward, 5'-AAGTGGCCAGTTGAAGAAGTGT-3'; reverse, 5'-CTCTACAGCTATATTGCCAGCCA-3'
miR-1301-3p	Forward, 5'-TTGCAGCTGCCTGGGA-3'; reverse, 5'-CTCTACAGCTATATTGCCAGCCA-3'
miR-126-5p	Forward, 5'-CATTATTACTTTTGGTACGCG-3'; reverse, 5'-CTCTACAGCTATATTGCCAGC-3'
miR-485-3p	Forward, 5'-GTCATACACGGCTCTCTCTCT-3'; reverse, 5'-CTCTACAGCTATATTGCCAGCCAC-3'
miR-4770	Forward, 5'-TGAGATGACACTGTAGCT-3'; reverse, 5'-CTCTACAGCTATATTGCC-3'
miR-101-3p	Forward, 5'-TACAGTACTGTGATAACTGAA-3'; reverse, 5'-CTCTACAGCTATATTGCC-3'
miR-221-3p	Forward, 5'-AGCTACATTGTCTGCTGGTTTC-3'; reverse, 5'-CTCTACAGCTATATTGCCAGCCAC-3'
miR-222-3p	Forward, 5'-AGCTACATCTGGCTACTGGGT-3'; reverse, 5'-CTCTACAGCTATATTGCCAGCC-3'
miR-134-5p	Forward, 5'-TGTGACTGTTGACCAGAGG-3'; reverse, 5'-CTCTACAGCTATATTGCCAGCCAC-3'
miR-26a-5p	Forward, 5'-TTCAAGTAATCCAGGATAGGCT-3'; reverse, 5'-CTCTACAGCTATATTGCCAGCC-3'
CUL2	Forward, 5'-CCGTTTCTCAGATATCTATGCT-3'; reverse, 5'-GTACTTGTCTTCTGACTCCA-3'
STRN3	Forward, 5'-AAGCATGGAATACCTACATCAG-3'; reverse, 5'-AGTTACCATATGAGCTGGA-3'
U6	Forward, 5'-GGATCAATACAGAGCAGATAAGC-3'; reverse, 5'-CTTTCTGAATTTGCGTGCC-3'
GAPDH	Forward, 5'-CTGGGTCACTGAGCACC-3'; reverse, 5'-AAGTGG TCGTTGAGGGCAATG-3'

gave informed consent, and this study was also permitted by the Ethics Committee of Shengjing Hospital of China Medical University.

Cell culture. Four CC cell lines (HeLa, SiHa, C33A, and CaSki) and one human cervical epithelial cell line (Ect1/E6E7) were purchased from the American Type Culture Collection (ATCC; USA). These cells were cultured in Dulbecco's modified Eagle's medium (DMEM; Invitrogen, USA) containing 10% fetal bovine serum (FBS; Invitrogen), 100 U/ml of penicillin, and 100 μ g/ml of streptomycin (Invitrogen). Cell culture was performed in a humidified atmosphere with 5% CO₂ at 37°C.

Cell transfection. HeLa and SiHa cells (1×10^6) were plated in 6-well plates. To silence LINC00997 or CUL2 expression, the short hairpin RNAs (shRNAs) targeting LINC00997 or CUL2 (sh-LINC00997#1/2 or sh-CUL2) and the negative control (sh-NC) were synthesized by GenePharma (Shanghai, China). The pcDNA3.1 vector overexpressing LINC00997 or CUL2 (pcDNA3.1/LINC00997 or pcDNA3.1/CUL2) with empty pcDNA3.1 vector as a control was designed and synthesized by Sangon (Shanghai, China). miR-574-3p mimics with NC mimics as a control and miR-574-3p inhibitor with NC inhibitor as a negative control were purchased from Sigma-Aldrich (MO). After these cells reached 70 to 80% confluence, cell transfection was conducted utilizing Lipofectamine 2000 (Invitrogen) according to the manufacturer's instructions. The efficiency of cell transfection was examined by reverse transcription-quantitative PCR (RT-qPCR) after 48 h.

RT-qPCR analysis. Total RNA was extracted from cells and tissues utilizing TRIzol reagent (Invitrogen), and reverse transcription into cDNA was conducted utilizing a PrimeScript RT reagent kit with a genomic DNA (gDNA) eraser (TaKaRa, Japan). Genomic DNA was extracted from tissues using the genomic DNA kit (Tiangen Biotech, Beijing, China) according to the manufacturer's protocols. The cDNA and genomic DNA were utilized for RT-qPCR, which was performed utilizing SYBR Premix Ex Taq II (TaKaRa) with the ABI 7500 real-time PCR system (ABI, Shanghai, China). The RNA expression levels and genomic DNA copy number levels of LINC00997, miR-574-3p, and CUL2 were determined utilizing the threshold cycle ($2^{-\Delta\Delta CT}$) method. Glyceraldehyde-3-phosphate dehydrogenase (GAPDH) was an internal control for the quantification of lncRNA and mRNA expression, while U6 was an internal reference for the quantification of miRNAs. LINE1 was set as an endogenous reference for the quantification of genomic DNA copy number. Primer sequences used in the study are listed in Table 1.

Western blot analysis. Total protein was extracted using radioimmunoprecipitation assay (RIPA) lysis buffer (Beyotime, Shanghai, China). Next, the protein was detached utilizing 10% SDS-PAGE and then was transferred to polyvinylidene difluoride (PVDF) membranes. The membranes were blocked with 5% skim milk for 2 h and then incubated with primary antibodies (Abcam, Cambridge, UK) overnight at 4°C. Afterwards, the membranes were probed by secondary antibodies (Abcam) for 2 h. Finally, the protein bands were detected and quantified using the ChemiDoc XRS+ system with Image Lab software (Bio-Rad, USA). The primary antibodies used were anti-LC3B (ab192890; 1:2,000), anti-beclin-1 (ab207612; 1:2,000), anti-CUL2 (ab166917; 1:1,000), anti-GAPDH (ab8245; 1:2,000), anti-ERK (ab32537; 1:1,000), anti-p-ERK (ab229912; 1:1,000), anti-p-JNK (ab124956; 1:1,000), anti-JNK (ab208035; 1:2,000), anti-p-p38 (ab178867; 1:1,000), and anti-p38 (ab59461; 1:1,000). The protein levels were normalized to GAPDH.

MTT assay. 3-(4,5-Dimethyl-2-thiazolyl)-2,5-diphenyl-2H-tetrazolium bromide (MTT) assays were conducted to examine the viability of CC cells. The transfected cells were plated onto 96-well plates (4×10^3 cells/well). Next, 20 μ l of MTT solution (Sigma-Aldrich) was added to each well for 2 h of incubation. Afterwards, 150 μ l of dimethyl sulfoxide (DMSO) was adopted to dissolve formazan crystal in each well. Finally, the optical density (OD) value at a wavelength of 490 nm was assessed using a Varioskan LUX multimode microplate reader (Thermo Fisher Scientific, USA).

Colony formation assay. The proliferation of CC cells was detected by colony formation assays. These cells were inoculated into 6-well plates (1×10^3 cells/well) with DMEM containing 10% FBS. After 2 weeks of incubation at 37°C, the cells were washed with phosphate-buffered solution (PBS; Thermo Fisher Scientific), fixed with 5% paraformaldehyde, and stained with 0.1% crystal violet (Beyotime) for 30 min. Finally, the colonies were washed with PBS, and the colonies containing over 50 cells were counted.

Transwell assays. Assays were conducted to examine the migration and invasion of HeLa and SiHa cells using Transwell chambers. For cell migration, the cells were added to the upper chambers (Millipore, USA) with serum-free DMEM. The lower chambers were supplemented with DMEM with 10% FBS. After 1 day of incubation, the cells that had migrated to the lower membranes were stained with crystal violet and quantitated in 5 randomly selected fields using a fluorescence microscope (Olympus, Japan). For cell invasion, the upper chambers were precoated with Matrigel (BD Biosciences, USA). Cells with transfection were placed in DMEM without FBS and then transferred to the upper chambers. After 30 min, the cells that had invaded the lower surface were fixed and stained with 0.1% FBS. Finally, the migrated and invaded cells were counted.

TEM observation. Transmission electron microscopy (TEM) was performed to probe the autophagy of HeLa and SiHa cells. The cells were fixed with 0.1 M sodium cacodylate solution containing 2.5% glutaraldehyde and 1% osmium tetroxide. After being rinsed and stained with PBS and 3% uranyl acetate solution, the cells were dehydrated with gradient alcohol. Subsequently, the cells were embedded in Epon-Araldite resin, and a Reichert ultramicrotome (Reichert-Jung, USA) was applied to cut embedded samples into slices. After being counterstained by 0.3% lead citrate, the slices were observed under an electron microscope (Philips, UK).

RNA pulldown assay. The RNA pulldown assay was performed in HeLa and SiHa cells utilizing a Pierce magnetic RNA-protein pulldown kit (Thermo Fisher Scientific) to explore the interaction between LINC00997 and candidate miRNAs. Biotinylated LINC00997 probe (LINC00997 probe-biotin) and the control (LINC00997 probe-nonbiotin) were purchased from GenePharma. The cells were lysed in RIPA buffer (Beyotime). Next, the lysate extracts were mixed with the biotinylated LINC00997 probes and then cultured with magnetic beads (Invitrogen) for 48 h at 4°C. After the RNA complexes on the beads were collected and purified, RT-qPCR was conducted to measure the expression of candidate miRNAs.

Luciferase reporter assay. The wild-type (Wt) or mutant (Mut) sequence of the CUL2 3' untranslated region (3' UTR) containing the miR-574-3p binding site was subcloned into pmirGLO vectors (Promega, USA) to construct pmirGLO-CUL2-Wt or pmirGLO-CUL2-Mut vector. The wild-type or mutated sequence of miR-574-3p was subcloned into pmirGLO vectors to construct miR-574-3p-Wt or miR-574-3p-Mut. The above-described constructed reporters were cotransfected with miR-574-3p mimics or pcDNA3.1/LINC00997 or their negative controls (NC mimics and pcDNA3.1) into HeLa and SiHa cells utilizing Lipofectamine 3000 reagent (Invitrogen). After 2 days of transfection, the luciferase reporter assay system (Promega) was employed to examine the luciferase activities of the reporters.

RIP assay. RNA-binding protein immunoprecipitation (RIP) assays were conducted to explore the relationship among LINC00997, miR-574-3p, and CUL2. HeLa or SiHa cells were lysed in RIP buffer. Next, the cell extract was cocultured with magnetic beads coated with human Ago2 antibody or the control IgG antibody (Abcam). After RNAs were purified, RT-qPCR was performed to quantify the enrichment of LINC00997 and CUL2 mRNA in CC cells transfected with miR-574-3p mimics or miR-574-3p inhibitor.

Subcellular fractionation assay. The subcellular fractionation assay was performed to determine the primary localization of LINC00997. A PARIS kit (Life Technologies, USA) was applied to isolate the cytoplasmic and nuclear RNAs based on the manufacturer's recommendations. GAPDH was a control for the cytoplasm, while U6 was an internal reference for the nucleus. RT-qPCR was conducted to measure the expression of LINC00997, GAPDH, and U6 in the cytoplasmic part and nuclear part of cells.

Statistical analysis. Statistical analysis was performed utilizing SPSS 21.0 software (SPSS, USA). The differences between two groups or among several groups were analyzed by Student's *t* test or one-way analysis of variance followed by Tukey's *post hoc* test. Data were expressed as the means \pm standard deviations (SD). Pearson's correlation analysis was used to identify gene expression correlation. A *P* value of <0.05 was regarded as statistically significant.

ACKNOWLEDGMENTS

There are no acknowledgments to be made.

There are no competing interests.

REFERENCES

1. Bray F, Ferlay J, Soerjomataram I, Siegel RL, Torre LA, Jemal A. 2018. Global cancer statistics 2018: GLOBOCAN estimates of incidence and mortality worldwide for 36 cancers in 185 countries. *CA Cancer J Clin* 68:394–424. <https://doi.org/10.3322/caac.21492>.
2. Arbyn M, Weiderpass E, Bruni L, de Sanjose S, Saraiya M, Ferlay J, Bray F. 2020. Estimates of incidence and mortality of cervical cancer in 2018: a worldwide analysis. *Lancet Glob Health* 8:e191–e203. [https://doi.org/10.1016/s2214-109X\(19\)30482-6](https://doi.org/10.1016/s2214-109X(19)30482-6).
3. Wentzensen N, Schiffman M. 2018. Accelerating cervical cancer control and prevention. *Lancet Public Health* 3:e6–e7. [https://doi.org/10.1016/S2468-2667\(17\)30242-6](https://doi.org/10.1016/S2468-2667(17)30242-6).
4. Cegla P, Burchardt E, Roszak A, Czepczynski R, Kubiak A, Cholewinski W. 2019. Influence of biological parameters assessed in [18F]FDG PET/CT on overall survival in cervical cancer patients. *Clin Nucl Med* 44:860–863. <https://doi.org/10.1097/RLU.0000000000002733>.
5. Small W, Jr, Bacon MA, Bajaj A, Chuang LT, Fisher BJ, Harkenrider MM, Jhingran A, Kitchener HC, Mileskin LR, Viswanathan AN, Gaffney DK. 2017. Cervical cancer: a global health crisis. *Cancer* 123:2404–2412. <https://doi.org/10.1002/cncr.30667>.
6. Rahmani Z, Mojarrad M, Moghbeli M. 2020. Long non-coding RNAs as the critical factors during tumor progressions among Iranian population: an overview. *Cell Biosci* 10:6. <https://doi.org/10.1186/s13578-020-0373-0>.

7. Li CH, Chen Y. 2016. Insight into the role of long noncoding RNA in cancer development and progression. *Int Rev Cell Mol Biol* 326:33–65. <https://doi.org/10.1016/bs.ircmb.2016.04.001>.
8. Gao YL, Zhao ZS, Zhang MY, Han LJ, Dong YJ, Xu B. 2017. Long noncoding RNA PVT1 facilitates cervical cancer progression via negative regulating of miR-424. *Oncol Res* 25:1391–1398. <https://doi.org/10.3727/096504017X14881559833562>.
9. Rui X, Xu Y, Jiang X, Ye W, Huang Y, Jiang J. 2018. Long non-coding RNA C5orf66-AS1 promotes cell proliferation in cervical cancer by targeting miR-637/RING1 axis. *Cell Death Dis* 9:1175. <https://doi.org/10.1038/s41419-018-1228-z>.
10. Peng L, Yuan X, Jiang B, Tang Z, Li GC. 2016. LncRNAs: key players and novel insights into cervical cancer. *Tumour Biol* 37:2779–2788. <https://doi.org/10.1007/s13277-015-4663-9>.
11. Du H, Chen Y. 2019. Competing endogenous RNA networks in cervical cancer: function, mechanism and perspective. *J Drug Target* 27:709–723. <https://doi.org/10.1080/1061186X.2018.1505894>.
12. Lou W, Ding B, Fu P. 2020. Pseudogene-derived lncRNAs and their miRNA sponging mechanism in human cancer. *Front Cell Dev Biol* 8:85. <https://doi.org/10.3389/fcell.2020.00085>.
13. Qi X, Zhang DH, Wu N, Xiao JH, Wang X, Ma W. 2015. ceRNA in cancer: possible functions and clinical implications. *J Med Genet* 52:710–718. <https://doi.org/10.1136/jmedgenet-2015-103334>.
14. Luan X, Wang Y. 2018. LncRNA XLOC_006390 facilitates cervical cancer tumorigenesis and metastasis as a ceRNA against miR-331-3p and miR-338-3p. *J Gynecol Oncol* 29:e95. <https://doi.org/10.3802/jgo.2018.29.e95>.
15. Shao S, Wang C, Wang S, Zhang H, Zhang Y. 2019. LncRNA STXBP5-AS1 suppressed cervical cancer progression via targeting miR-96-5p/PTEN axis. *Biomed Pharmacother* 117:109082. <https://doi.org/10.1016/j.biopha.2019.109082>.
16. Chang Y, Li N, Yuan W, Wang G, Wen J. 2019. LINC00997, a novel long noncoding RNA, contributes to metastasis via regulation of S100A11 in kidney renal clear cell carcinoma. *Int J Biochem Cell Biol* 116:105590. <https://doi.org/10.1016/j.biocel.2019.105590>.
17. Shi Z, Shen C, Yu C, Yang X, Shao J, Guo J, Zhu X, Zhou G. 2021. Long noncoding RNA LINC00997 silencing inhibits the progression and metastasis of colorectal cancer by sponging miR-512-3p. *Bioengineered* 12:627–639. <https://doi.org/10.1080/21655979.2021.1882164>.
18. Guo YJ, Pan WW, Liu SB, Shen ZF, Xu Y, Hu LL. 2020. ERK/MAPK signalling pathway and tumorigenesis. *Exp Ther Med* 19:1997–2007. <https://doi.org/10.3892/etm.2020.8454>.
19. Liu X, Yang Q, Yan J, Zhang X, Zheng M. 2019. LncRNA MNX1-AS1 promotes the progression of cervical cancer through activating MAPK pathway. *J Cell Biochem* 120:4268–4277. <https://doi.org/10.1002/jcb.27712>.
20. Wang XW, Zhang W. 2019. Long non-coding RNA cancer susceptibility candidate 2 inhibits the cell proliferation, invasion and angiogenesis of cervical cancer through the MAPK pathway. *Eur Rev Med Pharmacol Sci* 23:3261–3269. https://doi.org/10.26355/eurrev_201904_17687.
21. Xiao H, Liu Y, Liang P, Wang B, Tan H, Zhang Y, Gao J. 2018. TP53TG1 enhances cisplatin sensitivity of non-small cell lung cancer cells through regulating miR-18a/PTEN axis. *Cell Biosci* 8:23. <https://doi.org/10.1186/s13578-018-0221-7>.
22. Ye J, Chu C, Chen M, Shi Z, Gan S, Qu F, Pan X, Yang Q, Tian Y, Wang L, Yang W, Cui X. 2019. TROAP regulates prostate cancer progression via the WNT3/survivin signalling pathways. *Oncol Rep* 41:1169–1179. <https://doi.org/10.3892/or.2018.6854>.
23. Jiang L, Wang R, Fang L, Ge X, Chen L, Zhou M, Zhou Y, Xiong W, Hu Y, Tang X, Li G, Li Z. 2019. HCP5 is a SMAD3-responsive long non-coding RNA that promotes lung adenocarcinoma metastasis via miR-203/SNAI axis. *Theranostics* 9:2460–2474. <https://doi.org/10.7150/thno.31097>.
24. Qin G, Tu X, Li H, Cao P, Chen X, Song J, Han H, Li Y, Guo B, Yang L, Yan P, Li P, Gao C, Zhang J, Yang Y, Zheng J, Ju HQ, Lu L, Wang X, Yu C, Sun Y, Xing B, Ji H, Lin D, He F, Zhou G. 2020. Long noncoding RNA p53-stabilizing and activating RNA promotes p53 signaling by inhibiting heterogeneous nuclear ribonucleoprotein K deSUMOylation and suppresses hepatocellular carcinoma. *Hepatology* 71:112–129. <https://doi.org/10.1002/hep.30793>.
25. He F, Song Z, Chen H, Chen Z, Yang P, Li W, Yang Z, Zhang T, Wang F, Wei J, Wei F, Wang Q, Cao J. 2019. Long noncoding RNA PVT1-214 promotes proliferation and invasion of colorectal cancer by stabilizing Lin28 and interacting with miR-128. *Oncogene* 38:164–179. <https://doi.org/10.1038/s41388-018-0432-8>.
26. Kong F, Deng X, Kong X, Du Y, Li L, Zhu H, Wang Y, Xie D, Guha S, Li Z, Guan M, Xie K. 2018. ZFPM2-AS1, a novel lncRNA, attenuates the p53 pathway and promotes gastric carcinogenesis by stabilizing MIF. *Oncogene* 37:5982–5996. <https://doi.org/10.1038/s41388-018-0387-9>.
27. Levy JMM, Towers CG, Thorburn A. 2017. Targeting autophagy in cancer. *Nat Rev Cancer* 17:528–542. <https://doi.org/10.1038/nrc.2017.53>.
28. Antunes F, Erustes AG, Costa AJ, Nascimento AC, Bincoletto C, Ureshino RP, Pereira GJS, Smaili SS. 2018. Autophagy and intermittent fasting: the connection for cancer therapy? *Clinics (Sao Paulo)* 73:e814s. <https://doi.org/10.6061/clinics/2018/e814s>.
29. Zhang J, Liu L, Li J, Le TD. 2018. LncmiRSRN: identification and analysis of long non-coding RNA related miRNA sponge regulatory network in human cancer. *Bioinformatics* 34:4232–4240. <https://doi.org/10.1093/bioinformatics/bty525>.
30. Liu H, Lei C, He Q, Pan Z, Xiao D, Tao Y. 2018. Nuclear functions of mammalian microRNAs in gene regulation, immunity and cancer. *Mol Cancer* 17:64. <https://doi.org/10.1186/s12943-018-0765-5>.
31. Zhang P, Zhu J, Zheng Y, Zhang H, Sun H, Gao S. 2019. miRNA-574-3p inhibits metastasis and chemoresistance of epithelial ovarian cancer (EOC) by negatively regulating epidermal growth factor receptor (EGFR). *Am J Transl Res* 11:4151–4165.
32. Li W-C, Wu Y-Q, Gao B, Wang C-Y, Zhang J-J. 2019. MiRNA-574-3p inhibits cell progression by directly targeting CCND2 in colorectal cancer. *Biosci Rep* 39:BSR20190976. <https://doi.org/10.1042/BSR20190976>.
33. Wang M, Zhang R, Zhang S, Xu R, Yang Q. 2019. MicroRNA-574-3p regulates epithelial mesenchymal transition and cisplatin resistance via targeting ZEB1 in human gastric carcinoma cells. *Gene* 700:110–119. <https://doi.org/10.1016/j.gene.2019.03.043>.
34. Bai Y, Ding L, Baker S, Bai JM, Rath E, Jiang F, Wu J, Jiang H, Stuart G. 2016. Dissecting the biological relationship between TCGA miRNA and mRNA sequencing data using MMiRNA-Viewer. *BMC Bioinformatics* 17:336. <https://doi.org/10.1186/s12859-016-1219-y>.
35. Xu J, Fang Y, Wang X, Wang F, Tian Q, Li Y, Xie X, Cheng X, Lu W. 2016. CUL2 overexpression driven by CUL2/E2F1/miR-424 regulatory loop promotes HPV16 E7 induced cervical carcinogenesis. *Oncotarget* 7:31520–31533. <https://doi.org/10.18632/oncotarget.9127>.
36. Metzger R, Heukamp L, Drebbler U, Bollschweiler E, Zander T, Hoelscher AH, Warnecke-Eberz U. 2010. CUL2 and STK11 as novel response-predictive genes for neoadjuvant radiochemotherapy in esophageal cancer. *Pharmacogenomics* 11:1105–1113. <https://doi.org/10.2217/pgs.10.76>.
37. Michail O, Moris D, Theocharis S, Griniatsos J. 2018. Cullin-1 and -2 protein expression in colorectal cancer: correlation with clinicopathological variables. *In Vivo* 32:391–396. <https://doi.org/10.21873/invivo.11251>.
38. Peng W, Fan H. 2016. Long noncoding RNA CCHE1 indicates a poor prognosis of hepatocellular carcinoma and promotes carcinogenesis via activation of the ERK/MAPK pathway. *Biomed Pharmacother* 83:450–455. <https://doi.org/10.1016/j.biopha.2016.06.056>.
39. Han Y, Wu Z, Wu T, Huang Y, Cheng Z, Li X, Sun T, Xie X, Zhou Y, Du Z. 2016. Tumor-suppressive function of long noncoding RNA MALAT1 in glioma cells by downregulation of MMP2 and inactivation of ERK/MAPK signaling. *Cell Death Dis* 7:e2123. <https://doi.org/10.1038/cddis.2015.407>.
40. Zhang Y, Ma M, Liu W, Ding W, Yu H. 2014. Enhanced expression of long noncoding RNA CARLo-5 is associated with the development of gastric cancer. *Int J Clin Exp Pathol* 7:8471–8479.
41. Cicens J, Zalyte E, Rimkus A, Dapkus D, Noreika R, Urbonavicius S. 2017. JNK, p38, ERK, and SGK1 inhibitors in cancer. *Cancers (Basel)* 10:1. <https://doi.org/10.3390/cancers10010001>.
42. Li JH, Liu S, Zhou H, Qu LH, Yang JH. 2014. starBase v2.0: decoding miRNA-ceRNA, miRNA-ncRNA and protein-RNA interaction networks from large-scale CLIP-Seq data. *Nucleic Acids Res* 42:D92–D97. <https://doi.org/10.1093/nar/gkt1248>.
43. Bardou P, Mariette J, Escudié F, Djemiel C, Klopp C. 2014. jvenn: an interactive Venn diagram viewer. *BMC Bioinformatics* 15:293. <https://doi.org/10.1186/1471-2105-15-293>.